JACS
JOURNAL OF THE AMERICAN CHEMICAL SOCIETY
pubs.acs.org/JACS
Article

Topological Ordering of Memory Glass on Extended Length Scales

Sheng-Cai Zhu,*,¶ Gu-Wen Chen,¶ Dongzhou Zhang, Liang Xu, Zhi-Pan Liu, Ho-kwang Mao, and Qingyang Hu*

Cite This: J. Am. Chem. Soc. 2022, 144, 7414–7421
Read Online

ABSTRACT: Identifying ordering in non-crystalline solids has been a focus of natural science since the publication of Zachariasen's random network theory in 1932, but it still remains as a great challenge of the century. Literature shows that the hierarchical structures, from the short-range order of first-shell polyhedra to the long-range order of translational periodicity, may survive after amorphization. Here, in a piece of $AlPO_4$, or berlinite, we combine X-ray diffraction and stochastic free-energy surface simulations to study its phase transition and structural ordering under pressure. From reversible single crystals to amorphous transitions, we now present an unambiguous view of the topological ordering in the amorphous phase, consisting of a swarm of Carpenter low-symmetry phases with the same topological linkage, trapped in a metastable intermediate stage. We propose that the remaining topological ordering is the origin of the switchable "memory glass" effect. Such topological ordering may hide in many amorphous materials through disordered short atomic displacements.

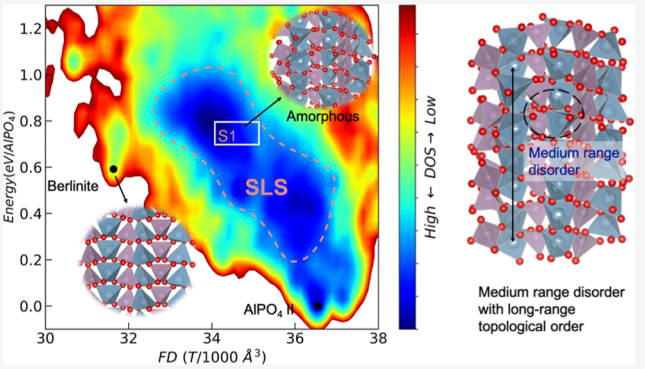

1. INTRODUCTION

According to atomic orderings of materials, all condensed matter can be divided into two types: crystalline and non-crystalline. The long-range ordering of crystalline solids consists of translational repetition of small- or medium-sized crystallographic unit cells that can be rigorously defined by one of the 230 space group symmetries. Non-crystalline (or amorphous) materials, however, lack such a translational ordering. Unlike the totally random gaseous state, amorphous materials still have a number of small- and medium-range orderings,[1] but the complications quickly mushroom with the size of clusters and become unmanageable. A clear description about the long-range ordering in non-crystalline solids is therefore crucial to understand the glass-forming process.

A widely cited theory for the formation of amorphous materials is Zachariasen's random network theory,[2] which is adequate for most network glasses under ambient pressure and fast temperature quenching but has seen exceptions for materials under pressure. Applying pressure creates another route to make non-crystalline solids by modulating the enthalpy.[3−8] For example, vitreous silica perfectly satisfies Zachariasen's four-point rules of glass formation. However, quartz and coesite upon pressure-induced amorphization (PIA) feature the edge-shared polyhedra, SiO_5 structural unit, and triple-linked O atoms,[6,8−10] all of which are not favored by Zachariasen's classical theory of a good glass former. Despite decades of research, the nature of PIA is still being debated. It was reported that some PIA turn out to be crystalline phase transition,[11] indicating that the consequent amorphous phase may lock up a portion of long-range ordering. An outstanding example is the fullerene crystal, which loses most of its short- to medium-range orderings upon room-temperature compression while sustaining the long-range translational order,[13] suggesting that pressure may freeze long-range topology but generate disordering within intermediate length scales. However, simultaneously applying high pressure and temperature, the same fullerene destroys its long-range periodicity, forming non-crystalline diamonds.[14,15] The method of PIA under cold compression, in fact, has left us an opportunity to study long-range ordering in amorphous materials through well-established crystallographic methods, for example, single-crystal diffraction.[16]

Long-range ordering has long been used to describe crystals. In contrast, from the perspective of a glass, Salmon et al.[17] thought long-range ordering covers more subjects than just translational periodicity. They presented the topological ordering concept related to the pair-distribution function (PDF) on much extended length scales and introduced it to describe the long-range ordering in network glass. Unlike

Received: February 14, 2022
Published: April 14, 2022

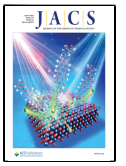

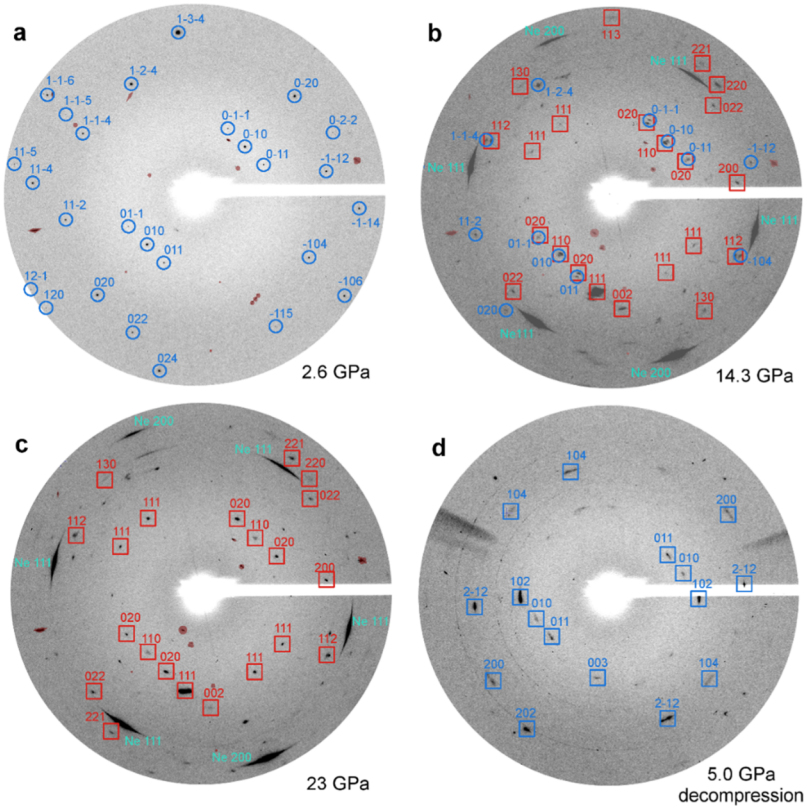

Figure 1. Selected single-crystal XRD patterns. The two-dimensional pattern was cut to exclude diamond diffraction spots. (a) Berlinite at 2.6 GPa. (b) Single-crystal berlinite and crushed poorly crystallized AlPO4 II at 14.3 GPa. (c) AlPO4 II at 23 GPa. (D) Recovered berlinite at 5.0 GPa after decompression. The weak diffraction rings in (d) are from WC seats.

crystallography, PDF cannot retrospectively reconstruct a long-range structure but is powerful to probe the network topology, which is the connectivity of structural motifs. Such a network topology has been observed in well-beyond medium ranges and has been gradually realized as an important description about long-range orderings in glasses.[17−19] In this work, we wish to characterize the hidden topological ordering in PIA materials, which will clarify its relation with crystal orientation and eventually describe the long-range ordering for non-crystalline solids.

Herein, we study the topological orderings of a non-crystalline solid starting from a crystal. We focus on the natural quartz homeotype berlinite (α-$AlPO_4$), which undergoes PIA and is the archetypal material for studying the memory glass transition. The PIA transition of berlinite takes place around 13 GPa,[4,5] and the amorphous $AlPO_4$ reverts to the original berlinite with identical crystal orientation upon releasing pressure.[20,21] Theoretical molecular dynamics simulations suggest that the memory effect is owing to the relatively short relaxation distance of O atoms in the PO_4 tetrahedron via a diffusionless transition.[22,23] However, the subsequent Raman scattering results argue that high-pressure glassy $AlPO_4$ is not a typical amorphous structure[12] but a poorly crystallized solid. The crystal structure is later identified to be the *Cmcm* space group (here abbreviated as $AlPO_4$ II) by X-ray diffraction (XRD).[24,25] Although the *Cmcm*-type phase is absent in the archetypal silica, it is found in other quartz homeotype compounds such as $GaPO_4$,[26,27] and the crystallization can be enhanced dramatically under moderate heating.[28] A recent theoretical study by Li at el.[29] found that berlinite has a structural transition at ∼19 GPa, where its bond length, angular distribution, and coordination number start to change and will smear the shape of PDFs. In spite of many experimental and simulation works, it is still controversial whether the high-pressure product is crystalline or amorphous. In this work, the ambiguity of the memory glass effect will be clarified by revealing the transition mechanism and the hidden topological orderings in amorphous $AlPO_4$, which will shed light on the ordering on extended length scales.

2. RESULTS

2.1. Revisiting the α-$AlPO_4$ to $AlPO_4$ II Transition through Single-Crystal Crystallography. We first conduct single-crystal XRD experiment, which is sensitive to both the crystal structure and orientation.[30−32] The crystal structures of $AlPO_4$ under high pressures are obtained at the beamline 13BM-C, GeoSoilEnviroCARS[33] of Advanced Photon Source, Argonne National Laboratory (Figure 1). The sample pressure is calibrated by the Raman edge of diamond.[34] Low-pressure XRD patterns of a pressurized single-crystal sample are unambiguously indexed to berlinite, in which the AlO_4 tetrahedron is corner-linked by four PO_4 tetrahedra (Figure S1 and Table S1). Increasing the pressure to 14.3 GPa generates a new set of diffraction spots and they coexist with berlinite (Figure 1b). We carefully checked the *d*-spacings of the newly emerged diffraction spots and found that they matched well with the high-pressure $AlPO_4$ II. However, the sample suffers poor crystallization. We observe crystal twinning or cracking into smaller grains when berlinite partially transforms into the AlPO4 II phase. Each grain has its own crystal orientation.

https://doi.org/10.1021/jacs.2c01717
J. Am. Chem. Soc. 2022, 144, 7414−7421

We notice that the diffraction intensity is substantially reduced due to the phase transition. Such a weakening indicates that the amorphous structure stays in harmony with the crystalline phases. Although our single-crystal XRD patterns confirm that berlinite is partially transformed into $AlPO_4$ II without requiring an isobaric heating process, the transition is sluggish in nature and, similar to the archetypal PIA in silica,[31] a portion of $AlPO_4$ samples might have been trapped into a number of intermediate structures on the potential energy surface (PES) (details are given in the next section). Beyond 23 GPa, the original berlinite disappears (Figure 1c), indicating that the phase transition has completed over a wide pressure range (~9 GPa).

We then release pressure and observe the re-emergence of berlinite (Figure 1d), reproducing the memory glass effect of the previous work.[20] The elongated diffraction spots are clear evidence of even worse crystal quality. Compared with the initial berlinite sample, the crystal orientation does not perfectly match with the original crystal. Specifically, many low *d*-spacing spots are too weak to be seen, and newly appeared diffraction spots such as 003 and 102 are absent in the original berlinite single crystal. However, we do observe spots such as 010 and 011, both of which memorize the original orientational information. There are two reasons for this occurrence. First of all, the recovered berlinite did not originate from one $AlPO_4$ crystallite, but multiple grains of the crushed crystallite stemmed from the previous transition. Second, it is possible that the amorphous $AlPO_4$ has inherited a portion of topological orderings from berlinite, and it performs a short-distance atomic reconstruction to memorize the berlinite structure and orientation upon decompression. The topology at the atomistic level and the mechanism that regulates PIA of $AlPO_4$ will be revealed by our computational simulations.

2.2. Exploring the Free-Energy Landscape. With the puzzles that arose from experiment, we perform global pathway searching over the free-energy landscape to link the initial state (berlinite) and the final state ($AlPO_4$ II) using the stochastic surface walking method (SSW).[35−37] The simulation is carried out in a 72-atom supercell, and more than 10^4 pairs of initial/final state are collected at 15 GPa by the high-dimensional neural-network (HDNN) potential.[38] Due to the expensive computational cost and the large number of reaction pathways, we employ a high-accuracy HDNN potential, which is an affordable method to construct the entire PES within a reasonable time, as well as to achieve a high computational accuracy. This method has successfully predicted the transition mechanism in compressed silica and graphite.[39,40] After the pathway collection, the transition state is located using the variable-cell double-ended surface walking approach,[37] and the candidate pathways are sorted by the height of energy barriers. The energy barrier is later recalculated and confirmed by the first-principles simulation using the Vienna ab initio simulation package.[41]

All the structures searched by the SSW are represented on the PES, projected on the axes of energy and framework density, namely, the number of Al/P atoms per 1000 Å^3 (shortened as FD in Figure 2). The PES with energy versus structural order parameter OP_6 is also shown in Figure S2 for reference. The PES consists of 13979 distinct structures and is colored by the probability density of state (DOS). For example, the more frequent a sample is sampled by the SSW algorithm, the higher the density will be. On the PES, the

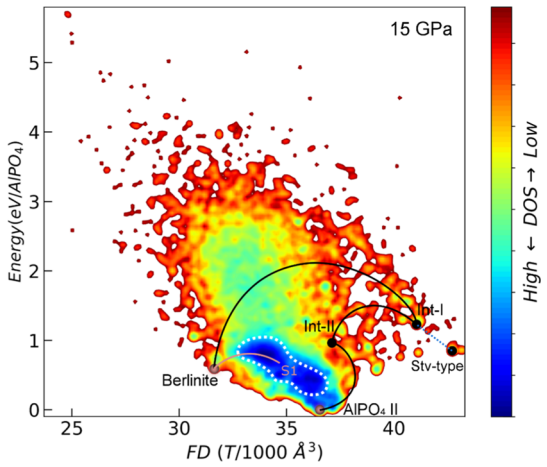

Figure 2. Global PES contour plot of $AlPO_4$ ($Al_{12}P_{12}O_{48}$) at 15 GPa. The *x* axis is the FD (the number of Al/P atoms per 1000 Å^3), the *y* axis is the total energy of minima with respect to the global minima phase ($AlPO_4$ II), and the color gradient indicates the probability DOS level of structures. The crystalline−crystalline route is connected by solid curves. Structural transition along the dotted curves overcomes a shallower kinetic barrier and involves a shorter atomic displacement but fails to reach the terminal phase. S1 is a structure in the high DOS swarm with a *P*1 space group. Stishovite-type $AlPO_4$ is not an energetically favored phase. Abbreviations: Stv, stishovite; Amor, amorphous phase.

locations of berlinite and $AlPO_4$ II are separated by a swarm of high-probability density structures. However, the crystalline−crystalline route connecting berlinite and the stable $AlPO_4$ II will bypass those high-density structures and transit indirectly toward the $AlPO_4$ II phase (solid curves in Figure 2), making it a less-probable event. The distribution of probability on the PES tells us that under room temperature and 15 GPa conditions, the sample has more chance to enter those structures encircled by white dashed lines in Figure 2. Throughout our in-depth pathway searching, the algorithm fails to find paths connecting them to the stable $AlPO_4$ II (e.g., S1—$AlPO_4$ II), implying that it is kinetically inhibited to complete a displacive transition from berlinite to $AlPO_4$ II out of the structures in the swarm. Below, we will go through both routes and reveal the topological orderings of structures in the swarm.

2.3. Breakdown of Topological Orderings in the Crystalline Transition. In the first place, we look at the special case of the crystalline−crystalline route toward $AlPO_4$ II. This route definitely breaks all long-range ordering of berlinite, but is at the cost of very sluggish transition kinetics. The pathway with the lowest kinetic barrier contains three crucial steps (Figure 3a) with descending barrier heights of 1.23, 0.25, and 0.16 eV/f.u. (f.u. = $AlPO_4$) and two intermediate structures (Int-I and Int-II). Increasing the pressure will lower the kinetic barriers (the inset of Figure 3a, also in Figure S3). Along with the reconstruction of long-range order, the signature spiral rings of polyhedra in berlinite (namely R1 and R2 in Figure 3b) are first distorted by shearing (berlinite to Int-I), then teared and recombined into dense-packed close-rings upon reaching $AlPO_4$ II. Structures along the path clearly show that the short-medium ordering of berlinite are reconstructed in the first step, where both Al and P atoms in Int-I are six-coordinated, leading to the rearrangement of long-range translation ordering in the following steps

https://doi.org/10.1021/jacs.2c01717
J. Am. Chem. Soc. 2022, 144, 7414−7421

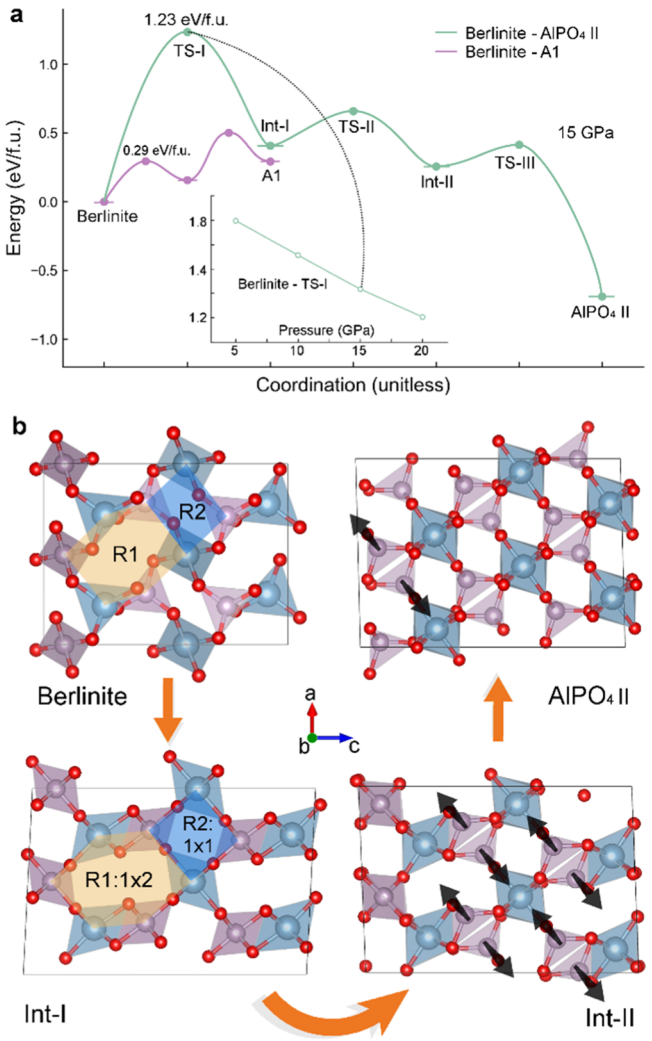

Figure 3. Kinetic barrier and structural evolution in compressed $AlPO_4$. (a) Energy barrier profile of α-$AlPO_4$ to $AlPO_4$ II and A1, corresponding to the points in Figure 2. The inset shows the height of the energy barrier at 5, 10, 15, and 20 GPa. (b) Structural evolution of α-$AlPO_4$ to $AlPO_4$ II, viewed from $[100]_\alpha$ or $[001]_{II}$. Two-thirds of P atoms transit from the octahedral to the tetrahedral interstitial in different directions with a negligible O movement, as shown by the arrow. Oxygen atoms associated with the rest of the one-third of P atoms have a much longer movement due to the periodic constraint in Int-II, as shown by the arrow in the last snapshot.

(Figures S4–S6). The atomic displacement is quantified by the Euclidian distance (defined in method). During the transition, the first step from berlinite to Int-I spans across the entire PES and its Euclidian distance are 8.6 Å, much longer than the following two steps (4.3 and 6.6 Å in the second and third steps). Nevertheless, both our experiment and simulations suggest that this route requires an appreciable amount of kinetic energy with multiple intermediate states. Unless applying heat, obtaining the crystalline $AlPO_4$ II is a less-probable event than other shorter-distance, lower-barrier transition pathways, which guide into the swarm with higher probability densities (Figure 2).

2.4. Description of Amorphous $AlPO_4$. The structures in the high-probability DOS area can be described as a swarm of low-symmetry structures (SLS). Their higher-probability DOS indicate that the onset kinetic barrier toward SLS is lower than the one from berlinite to Int-I, for example, from berlinite to a representative structure S1 in the SLS (added to Figure 3a). The missing pathway from S1 to $AlPO_4$ II echoes our experiment with the assumption that a portion of $AlPO_4$ is trapped en route to the final state. Compared to the crystalline–crystalline path, transition from berlinite to S1 features a much shorter displacement and only a fraction of atoms are involved in the structural transformation (Figure S7).

Our description about SLS is still insufficient because kinetics neither explain the memory transition effect nor the recovered crystal orientation. Inspired by Salmon,[17] we continue to calculate the PDF $G(r)$ (e.g., Al–O and P–O) of SLS. Obviously, a single triclinic structure taken from SLS produced a crystal-like pattern of $G(r)$ (Figure 4c,d). However, according to the energy landscape theory,[42] all the structures are unbiasedly sampled and the observed PDF can be approximated by averaging all structures in the SLS. We thus increase the number of sampled structures up to 812, which is a fraction of the entire SLS (Figure 4a), and the evolution of summed $G(r)$ has already shown qualitative changes. Specifically, the first sharp peak and nearly-zero $G(r)$ between the first and second peaks confirm that the structure has a well-established short-range order, which is defined by the first shell of polyhedral or simply Al–O or P–O bond lengths. The well-kept short-range order is also inferred from the bond-angle distribution of O–Al–O and O–P–O as well as the coordination number of cations (Al and P), see Figures S8 and S9, where the local polyhedral environments of P are almost the same as those of berlinite, while those of Al atoms are mixed of AlO_4 and AlO_6. However, a larger size of SLS reshapes $G(r)$ patterns between 3 and 10 Å, which is realized as the next-level structural organization of the abovementioned polyhedral blocks, or the medium-range order (Figure 4b). This is consistent with the angular distribution of O-centered angles, which signifies the connectivity of the two polyhedrons. Their bond-angle distribution flattens, indicating that the network of those polyhedrons is partially destroyed on medium-range length scales. It is worth noting that the medium-range order is investigated up to the longer edge of our simulation box, which is approximately 13 Å from all sampled structures. If an amorphous phase can be modeled by a $P1$ "crystal" with an infinitely large size of the unit cell, the translation orderings in SLS by the $P1$ symmetry are more likely a dwarfed amorphous structure. Putting all the $P1$ crystallites together, the nature of SLS is a non-translational, medium-range disordered solid with ordered polyhedral blocks. However, owing to the shorter atomic displacement and preferred kinetics, at least a portion of SLS revert to berlinite (e.g., S1—berlinite) once the reversal kinetics barrier is lowered, in response to decompression. Our experiments also hint that decompression rebuilds the long-rang ordering, both translational periodicity and orientation, which is consistent with previous single-crystal experiment in the literature.[20,21] There must be a fundamental layer of long-range ordering being kept in the SLS, defining the $AlPO_4$ glass just like the space group in crystal solids, and such an ordering will help recover long-range orderings such as translational periodicity and orientation under appropriate conditions.

2.5. Topological Ordering in Amorphous $AlPO_4$. The breakdown of crystalline symmetry under spontaneous strain has been documented by the crystal transition theory of Carpenter, who regarded that ferroelastic behavior corresponds to a normal group to subgroup topological projection.[43] On

https://doi.org/10.1021/jacs.2c01717
J. Am. Chem. Soc. 2022, 144, 7414–7421

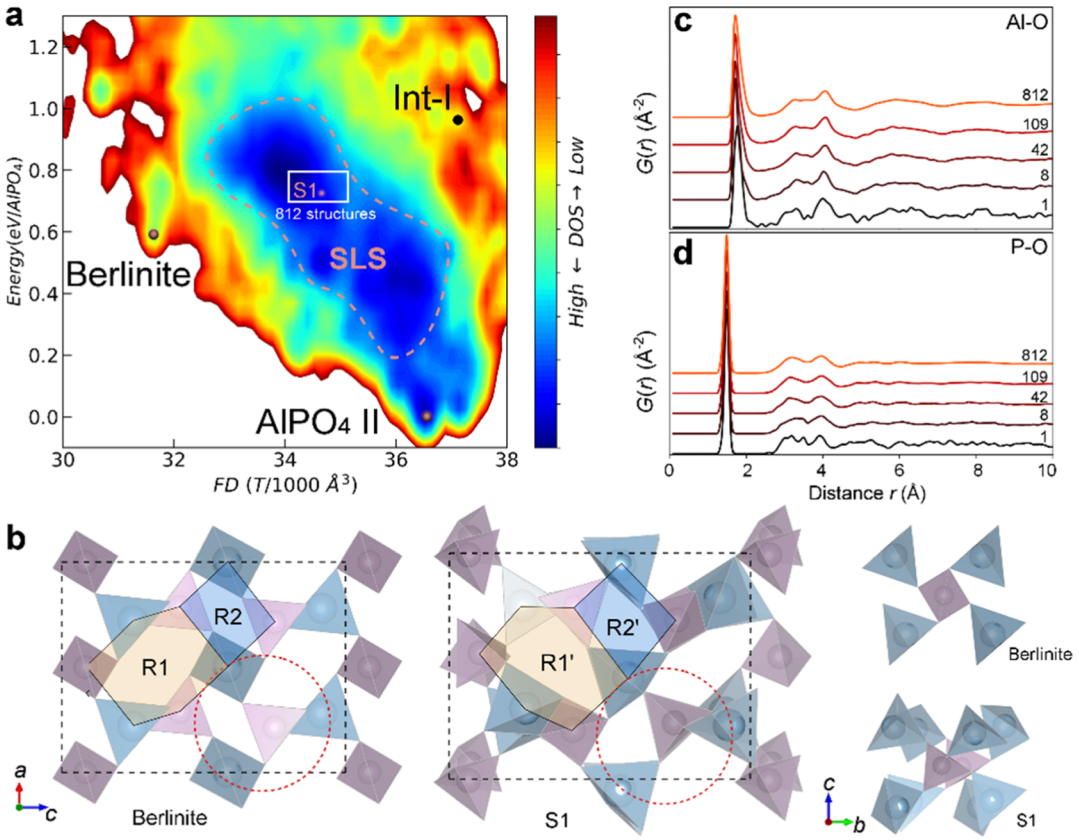

Figure 4. Topological orderings in amorphous $AlPO_4$. (a) Zoom-out PES showing the location of SLS. (b) Topology of berlinite and S1 from the SLS, viewed from the *b* axis. The spiral rings of R1 and R2 were distorted into R1′ and R2′ through polyhedral rotation. The medium-range structure in the red dashed ring is shown on the right, viewed from the *a* axis. (c,d) Evolution of the PDF of Al−O and P−O by varying the sampling size.

the basis of Carpenter's model, the symmetry of berlinite is lowered under strain, while in our experiment, the topological structures of non-crystalline $AlPO_4$ including the connectivity of building blocks, the spiral ring framework of berlinite, and the repetition of Al-/P- polyhedral are more or less kept. Our simulation clearly demonstrates that such a topological ordering is arranged along certain directions (Figure S10) and propagated by the simulation box. For example, from berlinite to S1 (Figure 4b), the rotation of polyhedral distorts the unit cell to the lowest triclinic lattice but the topological, atom−atom displacive paths are fully traceable, as recorded by our calculated transition pathway.

Berlinite's signature spiral rings (R1 and R2) are deformed arbitrarily, but its topology is well maintained in the SLS, for example, the S1 of Figure 4b, and more details are provided in Figure S11. This is in stark contrast to the intermediate states in the crystalline−crystalline route, where the spiral rings combine to closed rings. Although the spiraling features of R1 and R2 remain, the connectivity of the associated polyhedron is largely disordered as shown by the flattened angular distribution of X−O−X angles (X is Al or P). We therefore conclude that the amorphous $AlPO4_4$ is the extreme case of Carpenter-type crystalline transition, where a swarm of subgroup low-symmetry structures coexist, which can be projected to the normal group (e.g., berlinite) through a topological transition (e.g., following our calculated transition pathways). The set of topological transitions involves short displacements of atoms and are of first-order, by overcoming relatively lower-height barriers. The total excess energy for this transition can be expanded by the integral of spontaneous strains from Carpenter's crystalline transition theory.[44] The recovered crystal orientation will be highly dependent on the remaining topology,[45] for example, along the [001] axis on extended length scales (Figure S10).

3. DISCUSSION

Unlike the classic oxide glass of Zachariasen,[2] our results suggest the $AlPO_4$ memory glass prefers the description of a SLS consisting of low-symmetry crystallites, which also lead to the weakening and broadening of diffraction peaks. The SLS has a similar short-range ordering of berlinite or $AlPO_4$ II, but lacks a medium-range ordering. The long-range topological ordering, which describes the fundamental long-range structure of amorphous $AlPO_4$, is the key to the memory glass effect. As long as the topological ordering is kept, an amorphous solid is possible to recover to its corresponding crystal through a short atomic displacement. Here, the switchable crystalline−amorphous phase transition of $AlPO_4$ makes it a unique example for establishing this concept of long-range topological ordering in non-crystalline solids. A similar topological ordering may have occurred in many other PIA materials, although they possibly have much more complex topological structures.

It should be mentioned that the amorphous structures achieved through the route of PIA or thermal quenching are different. Whether a supercooled liquid crystallizes or vitrifies is largely controlled by the cooling rate.[46] A typical example is the formation of monoatomic metallic glass from ultrafast laser

https://doi.org/10.1021/jacs.2c01717
J. Am. Chem. Soc. 2022, 144, 7414−7421

cooling.[47] In contrast, increasing the pressurization rate in the process of PIA does not necessarily promote amorphization. For instance, the archetypal quartz silica crystalizes into a disordered metastable *d*-NiAs-type phase via gas-gun shock compression to 65 GPa.[48] Their experiment hints that the disordered phase has short-range and topological orderings, but it is neither a crystal nor an amorphous structure in nature. Shock compression generates pressure as well as heat. Therefore, contrary to cooling to vitrify a glass-forming material, a faster pressurization rate shortens atomic diffusion and may help maintain the topological ordering. We propose that pressure tends to partially destroy the medium-range and long-range translational orderings that manage the symmetry of a certain space group, but the destruction of topological ordering requires heating or long-time random diffusion of atoms.

4. CONCLUSIONS

In summary, this work combines in situ high-pressure single-crystal XRD and stochastic free-energy surface simulations to resolve the reversible crystalline−glass transition in $AlPO_4$. Not only we revisit the memory effect of the crystal structure and orientation under pressure herein but also we find that the amorphous phase inherits the long-range topological ordering from berlinite. This unique case of memory transition suggests that the building blocks of glass are organized by a more flexible and durable topological ordering on extended length scales, such that the experimentally observed glassy phase can be regarded as a swarm of Carpenter low-symmetry phases with the same topological linkage. Similar to the use of crystal space groups, it is possible to define an amorphous phase through its topological ordering, which readily interprets structural disordering in a wide range of materials.

■ ASSOCIATED CONTENT

Supporting Information

The Supporting Information is available free of charge at https://pubs.acs.org/doi/10.1021/jacs.2c01717.

Single-crystal experiment; details of SSW global optimization and pathway sampling methods; validation of high-pressure $AlPO_4$ HDNN potentials; DFT calculation details; atomic packing of $AlPO_4$ polymorphs; PES with structural order parameters; relative energies of the *Cmcm* phase as a function of pressure; O sublattice of berlinite, Int-I, and $AlPO_4$ II; phonon dispersion of Int-I and the heterogenous phase transition from Int-1 to $AlPO_4$ II; atomic projected displacement starting from berlinite; bond-angle distribution; coordination number analysis; and cation planar distance and selected structures taken from the SLS (PDF)

Accession Codes

CCDC 2162544 contains the supplementary crystallographic data for this paper. These data can be obtained free of charge via www.ccdc.cam.ac.uk/data_request/cif, or by emailing data_request@ccdc.cam.ac.uk, or by contacting The Cambridge Crystallographic Data Centre, 12 Union Road, Cambridge CB2 1EZ, UK; fax: +44 1223 336033.

■ AUTHOR INFORMATION

Corresponding Authors

Sheng-Cai Zhu − *School of Materials, Shenzhen Campus of Sun Yat-sen University, Shenzhen 518107, China;* orcid.org/0000-0003-3311-6723; Email: zhushc@mail.sysu.edu.cn

Qingyang Hu − *Center for High Pressure Science and Technology Advanced Research (HPSTAR), Beijing 100094, China; CAS Center for Excellence in Deep Earth Science, Guangzhou Institute of Geochemistry, Chinese Academy of Sciences, Guangzhou 510640, China;* orcid.org/0000-0002-2742-3017; Email: qingyang.hu@hpstar.ac.cn

Authors

Gu-Wen Chen − *School of Materials, Shenzhen Campus of Sun Yat-sen University, Shenzhen 518107, China*

Dongzhou Zhang − *Hawai'i Institute of Geophysics and Planetology, School of Ocean Earth Science and Technology, University of Hawai'i at Manoa, Honolulu, Hawaii 96822, United States;* orcid.org/0000-0002-6679-892X

Liang Xu − *National Key Laboratory of Shock Wave and Detonation Physics, Institute of Fluid Physics, China Academy of Engineering Physics, Mianyang 621900, China*

Zhi-Pan Liu − *Collaborative Innovation Center of Chemistry for Energy Material, Shanghai Key Laboratory of Molecular Catalysis and Innovative Materials, Key Laboratory of Computational Physical Science, Department of Chemistry, Fudan University, Shanghai 200433, China;* orcid.org/0000-0002-2906-5217

Ho-kwang Mao − *Center for High Pressure Science and Technology Advanced Research (HPSTAR), Beijing 100094, China*

Complete contact information is available at: https://pubs.acs.org/10.1021/jacs.2c01717

Author Contributions

¶S.-C.Z. and G.-W.C. contributed equally.

Notes

The authors declare no competing financial interest.

■ ACKNOWLEDGMENTS

This work was supported by NSFC (grant no: 21703004 and 42150101) and the Hundreds of Talents Program of Sun Yat-sen University, and CAEP Research Project (CX20210048). Q.H. was supported by the Tencent Xplorer Prize (XPLORER-2020-1013). We thank the Smithsonian National Museum of National History for the berlinite sample (catalog number: 106269 00). GeoSoilEnviroCARS was supported by the National Science Foundation (NSF)−Earth Sciences (EAR-1634415), and 13BM-C was partially supported by COMPRES under NSF Cooperative Agreement EAR 11-57758. We also acknowledge the use of computing resources from the Tianhe-2 Supercomputer.

■ REFERENCES

(1) Sheng, H. W.; Luo, W. K.; Alamgir, F. M.; Bai, J. M.; Ma, E. Atomic Packing and Short-to-Medium-Range Order in Metallic Glasses. *Nature* **2006**, *439*, 419−425.

(2) Zachariasen, W. H. The Atomic Arrangement in Glass. *J. Am. Chem. Soc.* **1932**, *54*, 3841−3851.

(3) Hemley, R. J.; Jephcoat, A. P.; Mao, H. K.; Ming, L. C.; Manghnani, M. H. Pressure-Induced Amorphization of Crystalline Silica. *Nature* **1988**, *334*, 52−54.

(4) Jayaraman, A.; Wood, D. L.; Maines, R. G. High-Pressure Raman Study of the Vibrational Modes in $AlPO_4$ and SiO_2 (α-Quartz). *Phys. Rev. B: Condens. Matter Mater. Phys.* **1987**, *35*, 8316−8321.

(5) Poswal, H. K.; Garg, N.; Somayazulu, M.; Sharma, S. M. Pressure-Induced Structural Transformations in the Low-Cristobalite Form of $AlPO_4$. *Am. Mineral.* **2013**, *98*, 285−291.
(6) Dmitriev, V. P.; Tolédano, P.; Torgashev, V. I.; Salje, E. K. H. Theory of Reconstructive Phase Transitions between SiO_2 Polymorphs. *Phys. Rev. B: Condens. Matter Mater. Phys.* **1998**, *58*, 11911−11921.
(7) Gamero-Castaño, M.; Torrents, A.; Valdevit, L.; Zheng, J.-G. Pressure-Induced Amorphization in Silicon Caused by the Impact of Electrosprayed Nanodroplets. *Phys. Rev. Lett.* **2010**, *105*, 145701.
(8) Zhang, H.; Tóth, O.; Liu, X.-D.; Bini, R.; Gregoryanz, E.; Dalladay-Simpson, P.; De Panfilis, S.; Santoro, M.; Gorelli, F. A.; Martoňák, R. Pressure-Induced Amorphization and Existence of Molecular and Polymeric Amorphous Forms in Dense SO_2. *Proc. Natl. Acad. Sci.* **2020**, *117*, 8736−8742.
(9) Badro, J.; Barrat, J.-L.; Gillet, P. Numerical Simulation of α-Quartz under Nonhydrostatic Compression: Memory Glass and Five-Coordinated Crystalline Phases. *Phys. Rev. Lett.* **1996**, *76*, 772−775.
(10) Badro, J.; Teter, D. M.; Downs, R. T.; Gillet, P.; Hemley, R. J.; Barrat, J.-L. Theoretical Study of a Five-Coordinated Silica Polymorph. *Phys. Rev. B: Condens. Matter Mater. Phys.* **1997**, *56*, 5797−5806.
(11) Onodera, Y.; Kohara, S.; Salmon, P. S.; Hirata, A.; Nishiyama, N.; Kitani, S.; Zeidler, A.; Shiga, M.; Masuno, A.; Inoue, H.; et al. Structure and Properties of Densified Silica Glass: Characterizing the Order within Disorder. *NPG Asia Mater.* **2020**, *12*, 85.
(12) Gillet, P.; Badro, J.; Varrel, B.; McMillan, P. F. High-Pressure Behavior in α-$AlPO_4$: Amorphization and the Memory-Glass Effect. *Phys. Rev. B: Condens. Matter Mater. Phys.* **1995**, *51*, 11262−11269.
(13) Wang, L.; Liu, B.; Li, H.; Yang, W.; Ding, Y.; Sinogeikin, S. V.; Meng, Y.; Liu, Z.; Zeng, X. C.; Mao, W. L. Long-Range Ordered Carbon Clusters: A Crystalline Material with Amorphous Building Blocks. *Science* **2012**, *337*, 825−828.
(14) Tang, H.; Yuan, X.; Cheng, Y.; Fei, H.; Liu, F.; Liang, T.; Zeng, Z.; Ishii, T.; Wang, M.-S.; Katsura, T.; et al. Synthesis of Paracrystalline Diamond. *Nature* **2021**, *599*, 605−610.
(15) Shang, Y.; Liu, Z.; Dong, J.; Yao, M.; Yang, Z.; Li, Q.; Zhai, C.; Shen, F.; Hou, X.; Wang, L.; et al. Ultrahard Bulk Amorphous Carbon from Collapsed Fullerene. *Nature* **2021**, *599*, 599−604.
(16) Machon, D.; Meersman, F.; Wilding, M. C.; Wilson, M.; McMillan, P. F. Pressure-Induced Amorphization and Polyamorphism: Inorganic and Biochemical Systems. *Prog. Mater. Sci.* **2014**, *61*, 216−282.
(17) Salmon, P. S.; Martin, R. A.; Mason, P. E.; Cuello, G. J. Topological versus Chemical Ordering in Network Glasses at Intermediate and Extended Length Scales. *Nature* **2005**, *435*, 75−78.
(18) Mavračić, J.; Mocanu, F. C.; Deringer, V. L.; Csányi, G.; Elliott, S. R. Similarity Between Amorphous and Crystalline Phases: The Case of TiO_2. *J. Phys. Chem. Lett.* **2018**, *9*, 2985−2990.
(19) Li, N.; Ching, W.-Y. Structural, Electronic and Optical Properties of a Large Random Network Model of Amorphous SiO2 Glass. *J. Non-Cryst. Solids* **2014**, *383*, 28−32.
(20) Kruger, M. B.; Jeanloz, R. Memory Glass: An Amorphous Material Formed from $AlPO_4$. *Science* **1990**, *249*, 647−649.
(21) Polian, A.; Grimsditch, M.; Philippot, E. Memory Effects in Pressure Induced Amorphous $AlPO_4$. *Phys. Rev. Lett.* **1993**, *71*, 3143−3145.
(22) Tse, J. S.; Klug, D. D. Structural Memory in Pressure-Amorphized $AlPO_4$. *Science* **1992**, *255*, 1559−1561.
(23) Chaplot, S. L.; Sikka, S. K. Molecular-Dynamics Simulation of Pressure-Induced Crystalline-to-Amorphous Transition in Some Corner-Linked Polyhedral Compounds. *Phys. Rev. B: Condens. Matter Mater. Phys.* **1993**, *47*, 5710−5714.
(24) Sharma, S. M.; Garg, N.; Sikka, S. K. High-Pressure x-Ray-Diffraction Study of α-$AlPO_4$. *Phys. Rev. B: Condens. Matter Mater. Phys.* **2000**, *62*, 8824−8827.
(25) Sharma, S. M.; Garg, N.; Sikka, S. K. High Pressure Phase Transformations in α-$AlPO_4$: An x-Ray Diffraction Investigation. *J. Phys.: Condens. Matter* **2000**, *12*, 6683−6692.
(26) Ming, L. C.; Nakamoto, Y.; Endo, S.; Chio, C. H.; Sharma, S. K. Phase Transformations of α-Cristobalite $GaPO_4$ at Pressures up to 52 GPa. *J. Phys.: Condens. Matter* **2007**, *19*, 425202.
(27) Peters, M. J.; Grimsditch, M.; Polian, A. High-Pressure Raman Scattering from GaPO4. *Solid State Commun.* **2000**, *114*, 335−340.
(28) Badro, J.; Itié, J. P.; Polian, A. On the High-Pressure Phase Transition in $GaPO_4$. *Eur. Phys. J. B* **1998**, *1*, 265−268.
(29) Li, N.; Hu, H.; Guo, F.; Tao, H. Uncovering the Phase Transition of Berlinite (α-AlPO4) under High Pressure: Insights from First-Principles Calculations. *J. Wuhan Univ. Technol., Mater. Sci. Ed.* **2021**, *36*, 248−254.
(30) Hu, Q. Y.; Shu, J.-F.; Yang, W. G.; Park, C.; Chen, M. W.; Fujita, T.; Mao, H.-K.; Sheng, H. W. Stability Limits and Transformation Pathways of α -Quartz under High Pressure. *Phys. Rev. B* **2017**, *95*, 104112.
(31) Hu, Q. Y.; Shu, J.-F.; Cadien, A.; Meng, Y.; Yang, W. G.; Sheng, H. W.; Mao, H.-K. Polymorphic Phase Transition Mechanism of Compressed Coesite. *Nat. Commun.* **2015**, *6*, 6630.
(32) Ernok, A.; Ballaran, T. B.; Caracas, R.; Miyajima, N.; Bykova, E.; Prakapenka, V.; Liermann, H.-P.; Dubrovinsky, L. Pressure-Induced Phase Transitions in Coesite. *Am. Mineral.* **2014**, *99*, 755−763.
(33) Xu, J.; Zhang, D.; Tkachev, S. N.; Dera, P. K. Partnership for EXtreme Xtallography (PX 2)—A State-of-the-Art Experimental Facility for Extreme-Conditions Crystallography: A Case Study of Pressure-Induced Phase Transition in Natural Ilvaite. *Matter Radiat. Extremes* **2022**, *7*, 028401.
(34) Hu, Q.; Mao, H.-k. Born's Valence Force-Field Model for Diamond at Terapascals: Validity and Implications for the Primary Pressure Scale. *Matter Radiat. Extremes* **2021**, *6*, 068403.
(35) Shang, C.; Liu, Z.-P. Stochastic Surface Walking Method for Structure Prediction and Pathway Searching. *J. Chem. Theory Comput.* **2013**, *9*, 1838−1845.
(36) Shang, C.; Zhang, X.-J.; Liu, Z.-P. Stochastic Surface Walking Method for Crystal Structure and Phase Transition Pathway Prediction. *Phys. Chem. Chem. Phys.* **2014**, *16*, 17845−17856.
(37) Zhang, X.-J.; Liu, Z.-P. Variable-Cell Double-Ended Surface Walking Method for Fast Transition State Location of Solid Phase Transitions. *J. Chem. Theory Comput.* **2015**, *11*, 4885−4894.
(38) Huang, S.-D.; Shang, C.; Zhang, X.-J.; Liu, Z.-P. Material Discovery by Combining Stochastic Surface Walking Global Optimization with a Neural Network. *Chem. Sci.* **2017**, *8*, 6327−6337.
(39) Zhu, S.-c.; Hu, Q.-y. Unraveling the Structural Transition Mechanism of Room-Temperature Compressed Graphite Carbon. *Phys. Chem. Chem. Phys.* **2021**, *23*, 20560−20566.
(40) Zhu, S.-c.; Yan, X.-z.; Liu, J.; Oganov, A. R.; Zhu, Q. A Revisited Mechanism of the Graphite-to-Diamond Transition at High Temperature. *Matter* **2020**, *3*, 864−878.
(41) Kresse, G.; Furthmüller, J. Efficient Iterative Schemes for Ab Initio Total-Energy Calculations Using a Plane-Wave Basis Set. *Phys. Rev. B: Condens. Matter Mater. Phys.* **1996**, *54*, 11169.
(42) Wales, D. J. Energy Landscapes. *Atomic clusters and nanoparticles. Agregats atomiques et nanoparticules*; Springer Berlin Heidelberg: Berlin, Heidelberg, 2001; pp 437−507.
(43) Carpenter, M. A.; Salje, E. K. H.; Graeme-Barber, A. Spontaneous Strain as a Determinant of Thermodynamic Properties for Phase Transitions in Minerals. *Eur. J. Mineral.* **1998**, *10*, 621−691.
(44) Carpenter, M. A.; Salje, E. K. H. Elastic Anomalies in Minerals Due to Structural Phase Transitions. *Eur. J. Mineral.* **1998**, *10*, 693−812.
(45) Redfern, S. T.; Graeme-Barber, A.; Salje, E. Thermodynamics of Plagioclase III: Spontaneous Strain at the I-1-P-1 Phase Transition in Ca-Rich Plagioclase. *Phys. Chem. Miner.* **1988**, *16*, 157−163.
(46) Turnbull, D. Under What Conditions Can a Glass Be Formed? *Contemp. Phys.* **1969**, *10*, 473−488.
(47) Zhong, L.; Wang, J.; Sheng, H.; Zhang, Z.; Mao, S. X. Formation of Monatomic Metallic Glasses through Ultrafast Liquid Quenching. *Nature* **2014**, *512*, 177−180.

https://doi.org/10.1021/jacs.2c01717
J. Am. Chem. Soc. 2022, 144, 7414−7421

(48) Tracy, S. J.; Turneaure, S. J.; Duffy, T. S. Structural Response of α-Quartz under Plate-Impact Shock Compression. *Sci. Adv.* **2020**, *6*, No. eabb3913.

https://doi.org/10.1021/jacs.2c01717
J. Am. Chem. Soc. 2022, 144, 7414−7421